The impact of cementing technique in polished taper fit hip stems

a modelling analysis of implant-cement interface

From University of Leeds, Leeds, UK

Cite this article:
Bone Joint Res 2025;14(7):
642–655.

DOI: 10.1302/2046-3758.
147.BJR-2024-0408.R1

Correspondence should be sent to Bernard H. van Duren
b.h.vanduren@gmail.com

B. H. van Duren,[1,2] M. Taufiqurrakhman,[2] A. Jones,[3] M. Higgins,[1] A. R. Manktelow,[1] B. V. Bloch,[1,4] H. Pandit[2]

[1]Nottingham Elective Orthopaedic Services, Nottingham University Hospitals NHS Trust, Nottingham, UK
[2]Leeds Institute of Rheumatic and Musculoskeletal Medicine, University of Leeds, Leeds, UK
[3]School of Mechanical Engineering, University of Leeds, Leeds, UK
[4]University of Nottingham, School of Medicine, Nottingham, UK

Aims

Cemented polished taper fit (PTF) stems are the femoral implant of choice for total hip arthroplasty (THA) in many locations worldwide. There is increasing evidence that periprosthetic fracture may be the single major contributor to reoperation with these stems. The aim of this study was to demonstrate how mismatches at the implant-cement interface may occur and the subsequent effect of these incongruities on the contacting area and the forces transmitted to the cement mantle.

Methods

A parametric equation-based model was developed to determine the contact mismatch relative to axial stem rotations. This model was also used to calculate the restoration of contact surface area with stem subsidence for both a dual-taper and triple-taper geometry. A finite element analysis (FEA) was used to compare the effects of reduced contact area due to the incongruent hip implant-cement interface.

Results

The contact model showed a large decrease in surface contact area with even only a small rotation going from 100% at 0° to 50.00% at 2.5° for the dual-taper geometry, and from 100% at 0° to 50.20% at 2.5° for the triple-taper geometry. There was a gradual but small ongoing decrease in contact surface with increasing rotation for both the dual-taper and triple-taper geometries. For both taper designs, there was an increase in contact surface area with an increase in subsidence resulting in contact for up to a 5° mismatch being restored with 2 mm subsidence. FEA showed that with increasing mismatches and consequent contact area reduction, there was an increase in von Mises stress in the implant-cement interface of up to 235%.

Conclusion

With increasing mismatch, there was an increase in maximum stresses, total strain, and subsidence in the cement mantle, highlighting the importance of achieving an optimal implant-cement interface at the time of implantation of cemented PTF femoral stems.

Article focus

- This study aims to demonstrate the consequences of reduction in contact surface area at the implant-cement interface of PTF stems that potentially occur at the time of cementing.
- We hypothesized that a mismatch at the stem-cement interface contributes to increased pressure within the cement

Bone & Joint Research

mantle of polished taper fit femoral stems.

Key messages

- Small rotational movements can result in large (approximately 50%) decreases in cement-implant contact surface area.
- Simulation showed that these decreases in contact area can increase the maximal stresses in the cement mantle by up to 200%.
- This study highlights the importance of achieving an optimal implant-cement interface at the time of implantation.

Strengths and limitations

- A strength of this study is that it highlights factors within a surgeon's control to achieve an optimal cement mantle.
- A limitation is its use of simplified modelling techniques, which do not account for all possible variables.

Introduction

Implant choice and surgical technique are two key aspects of total hip arthroplasty (THA), which are within the control of the surgeon to affect a satisfactory clinical outcome for their patients.[1] Cemented polished taper fit (PTF) stems are the stem of choice in many locations worldwide.[2,3] There is growing evidence around an increased risk of periprosthetic fracture (PPF) with PTF stems over composite beam or uncemented stems.[4-10] However, a clear explanation for these observations has yet to be established. Whether this increased risk of PPF can be attributed to the taper fit philosophy as a whole, or only certain stem designs within this group, is unclear. Differences in the incidence of PPF have been noted when comparing current designs. Differences in material properties, surface finish, cement viscosity, and implant geometry have been suggested as possible causes.[11-14]

PTF stems are designed for an even distribution of forces to bone using an even cement mantle. Taper fit relies on a large contact surface area to distribute forces, maintained over time by controlled stem subsidence.[15] It follows that reducing this contact area or interruptions to its uniformity leads to both increased contact pressure as well as less optimal force distribution, which in turn increases the risk of fracture. The implant-cement interface plays a crucial role in the function of PTF stems. Contact mismatch at the cement implant interface potentially occurs either early on, related to improper surgical technique, or later on in the lifespan of the implant with cement creep damage and plastic deformation of the cement mantle.[16-18]

During cementing, the PTF stem is inserted into the cement mantle to the desired position. While the cement is curing, it spends some time in a plastic (pre-cured) state, meaning that changes/adjustments or movement when detaching the stem introducer and/or leg movement from the assistant during this period will create permanent shape changes in the surface, which could risk compromising the fit of the cement mantle. PTF stems use an interference fit to secure the stem within the cement mantle by creating a large contact area for the transfer of forces.[19] The 'load-transfer' (load transfer from stem to bone via cement mantle) generates stresses in the materials and at their interfaces, with the likelihood of mechanical failure depending on the stress levels relative to the material strengths.[20] A non-conforming cement mantle and reduction in contact area is potentially introduced at the time of stem insertion before the cement has cured. We hypothesize that a mismatch at the stem/cement interface leads to an uneven distribution of pressure on the cement mantle, leading to regions of the cement mantle transferring increased load and subsequently resulting in these areas being more likely to reach the point of failure.

The impact of reduction in contact surface area at the implant-cement interface, under stem rotation, has not been previously investigated. This study aims to demonstrate the reduction in contact surface area at the implant-cement interface with stem rotation using two methods: 1) an analytical cross-sectional model which assumes perfect plastic behaviour, and 2) finite element analysis (FEA) which includes elastic response. In addition, the ability of cemented PTF stems to compensate for a reduction in implant-cement mantle surface area under loading conditions was also explored. The degree to which stem subsidence can restore the contact surface area was explored using the same two models. The effect of implant-cement interface mismatch on the contacting area and the forces transmitted to the cement mantle was quantified using the FEA model.

Methods

Cross-sectional contact model

To demonstrate the reduction in implant-cement contact area due to the degree of incongruity between the implant and cement mantle geometry, a cross-sectional model was used. The cross-sectional geometry of a stem was described using a parametric function (Equation 1) to define eight shape components consisting of four radii and four edges. The shape components were defined by parameter 't', which was varied from 0 to 8 in the equations, resulting in points describing the outline of the stem in a single axial cross-section. In this model, 'w' represents half the width (medial-lateral) of the stem, 'd1' and 'd2' are the thicknesses (anterior-posterior) of the stem medially and laterally, respectively, and 'r1' to 'r4' are the radii at the cross-sectional corners of the stem (Figure 1).

Equation 1 was used to generate point clouds (t was varied at increments of 0.01, resulting in 800 points describing the stem cross-section) iteratively through rotational positions of the stem. To determine the points remaining in contact with the cement mantle, a second copy of the point cloud at 0° was used to describe the cement mantle. At 0°, the point clouds were coincident, representing perfect contact. With rotation of the point clouds representing the femur, remaining contact points could be calculated by subtracting the points which are within the bounds of the original cement mantle and previous stem positions (Figure 1). Rotational and translational mismatches were simulated with variations in origin relative to the stem to mimic mismatches during cementing (to account for designs where the stem introducer is not mounted along the axis of the taper) or cement fatigue with torsional forces pivoting around the medial calcar/cement mantle.

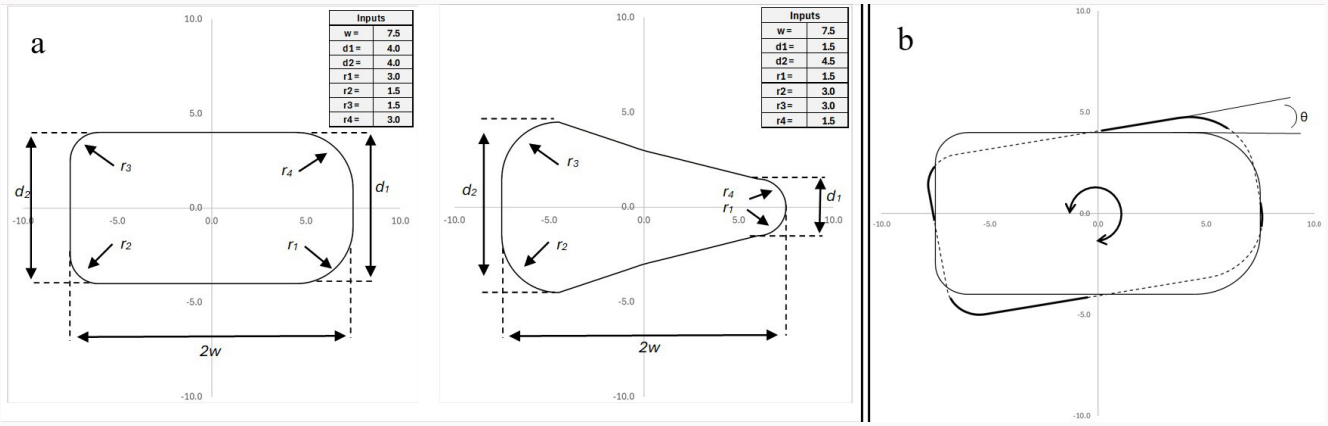

Fig. 1

a) Examples of dual-taper and triple-taper stem cross-sectional geometry models with respective parameters, where w is the width (medial-lateral) of the stem, d_1 and d_2 are the thickness (anterior-posterior) of the stem medially and laterally respectively, and r_1 and r_2 are the radii at the cross-sectional corners of the stem taper. b) Illustration of the effect of rotation on cross-sectional contact with the solid line representing the cement mantle, θ the angle of rotation, the bold lines the regions of the stem still in contact with cement, and the dashed lines the areas that are no longer in contact due to rotation.

$$f(t)=\begin{cases}\{w,-(d1-r4)(2t-1)\} & 0.0\le t\le 0.5\\ \{w,-(d1-r1)(2t-1)\} & 0.5<t\le 1.0\\ \left\{w-r1+r1.cos\left(\frac{1}{2}\pi(t-1)\right),-d1+r1-r1.sin\left(\frac{1}{2}\pi(t-1)\right)\right\} & 1.0<t\le 1.5\\ \left\{w-r1+r1.cos\left(\frac{1}{2}\pi(t-1)\right),-d1+r1-r1.sin\left(\frac{1}{2}\pi(t-1)\right)\right\} & 1.5<t\le 2.0\\ \{-(w-r1)(2t-5),\ -(d1+(t-2)(d2-d1))\} & 2.0<t\le 2.5\\ \{-(w-r2)(2t-5),\ -(d1+(t-2)(d2-d1))\} & 2.5<t\le 3.0\\ \left\{-w+r-r2.sin\left(\frac{1}{2}\pi(t-3)\right),-d2+r2-r2.cos\left(\frac{1}{2}\pi(t-3)\right)\right\} & 3.0<t\le 3.5\\ \left\{-w+r2-r2.sin\left(\frac{1}{2}\pi(t-3)\right),-d2+r2-r2.cos\left(\frac{1}{2}\pi(t-3)\right)\right\} & 3.5<t\le 4.0\\ \{-w,(d2-r2)(2t-9)\} & 4.0<t\le 4.5\\ \{-w,(d2-r3)(2t-9)\} & 4.5<t\le 5.0\\ \left\{-w+r3-r3.cos\left(\frac{1}{2}\pi(t-5)\right),d2-r3+r3.sin\left(\frac{1}{2}\pi(t-5)\right)\right\} & 5.0<t\le 5.5\\ \left\{-w+r3-r3.cos\left(\frac{1}{2}\pi(t-5)\right),d2-r3+r3.sin\left(\frac{1}{2}\pi(t-5)\right)\right\} & 5.5<t\le 6.0\\ \{(w-r3)(2t-13),\ (d2-(t-6)(d2-d1))\} & 6.0<t\le 6.5\\ \{(w-r4)(2t-13),\ (d2-(t-6)(d2-d1))\} & 6.5<t\le 7.0\\ \left\{w-r4+r4.sin\left(\frac{1}{2}\pi(t-7)\right),d2-r4+r4.cos\left(\frac{1}{2}\pi(t-7)\right)\right\} & 7.0<t\le 7.5\\ \left\{w-r4+r4.sin\left(\frac{1}{2}\pi(t-7)\right),d2-r4+r4.cos\left(\frac{1}{2}\pi(t-7)\right)\right\} & 7.5<t\le 8.0\end{cases}$$

Equation 1. Parametric equation used to describe cross-sectional geometry as a function of the parameter 't', where 'w' is the width (medial-lateral) of the stem, 'd_1' and 'd_2' are the thickness (anterior-posterior) of the stem medially and laterally, respectively, and r_1 to r_4 are the radii at the cross-sectional corners of the stem taper. These parameters correspond to those illustrated in Figure 1.

Effect of subsidence on contact area

An advantage of the cemented PTF stem is that it can compensate for an amount of implant-cement mantle mismatch through subsidence. This occurs with deformation of the contact areas, meaning that a broader section of the stem taper will increase contact with the cement mantle (Figure 2). The change in cross-sectional geometry (δ) with subsidence can be derived from the implant taper (θ) and the subsidence (s): $\delta = s.\tan\theta$.

To model this, the stem was moved by a set amount such that the area in contact for a particular rotation was a consequence of the taper. The model calculated the implant's cross-sectional geometry at the cement mantle level when including subsidence by adding the change in profile (δ) to 'w', 'd1', and 'd2', as well as to the 'r1' to 'r4' parameters (Figure 2). Using these new parameters, the contact points were recalculated with the retained cement mantle. To model the effect of this compensation, subsidence ranges, including 0.5 mm, 1.0 mm, 1.5 mm, and 2.0 mm, were modelled based on Baryeh and Sochart,[21] who in their meta-analysis reported a mean subsidence of cemented PTF stems at one, two, five, and ten years of 0.97 mm, 1.07 mm, 1.47 mm, and 1.61 mm, respectively.

Assumptions made in this model were, firstly, that the cement underwent perfect plastic deformation where there was contact on rotation of the stem. Time-dependent viscous behaviour of cement, potentially allowing it to fill gaps created by stem rotation, were not modelled. Secondly, the cross-sectional geometry was based on estimated measurements and did not represent true dimensions of actual implants. Finally, the cross-sectional geometry was assumed to be proportional with the taper along the length of the stem, and as such, the contact percentage could be applied along the length of the stem.

Finite element model

Computer-aided design (CAD) models of the cross-sections (dual-taper and triple-taper) of 100 mm in length and a taper angle of 7° within a cylindrical bone cement mantle were created using SolidWorks 2022 SP3.1 version (Dassault Systèmes, France). The distance between the proximal aspect of the cement restrictor was assumed to be 10 mm distal to the tip of the stem. A 2 mm void was modelled distal to the tip of the stem to simulate the use of a stem centralizer.

To simulate the effect of mismatches between implant and cement mantle, the hip stems were modelled at a rotation of 2.5° and 5°, representing geometrical mismatches, and compared to 0° (neutral), representing a fully conforming interface (Figure 3). The stem model was assembled and rotated within the solid cement model using SolidWorks, and the cement was cut by the stem geometry through a subtract feature before finite element meshing. This approach aimed to replicate the perfectly plastic deformation (pre-curing) of the model.

FEA was used to compare the effects of reduced contact area due to the incongruent hip stem-cement mantle interface. An overview of the material properties used is given in Table I. Static structural module in Ansys Workbench software version 2022 (Ansys, USA) was used in this study

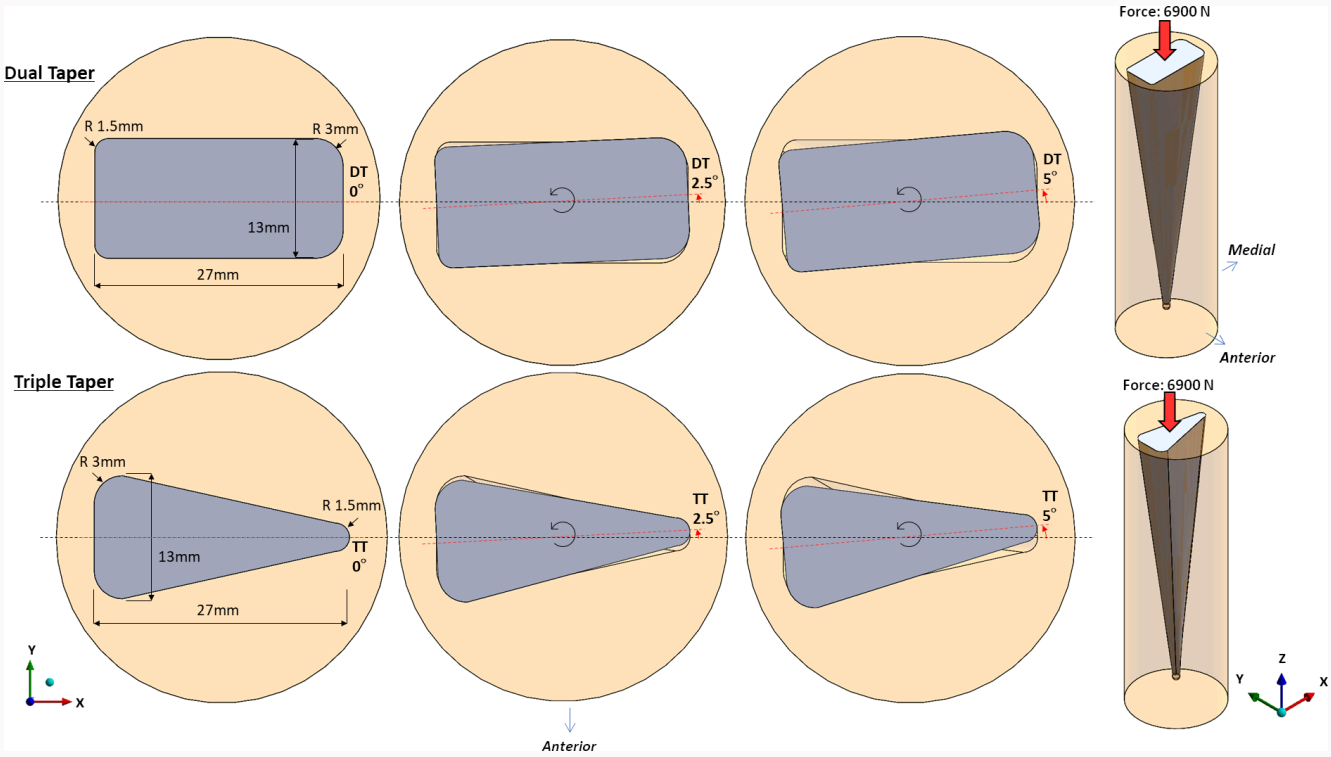

Fig. 2
Computer-aided design (CAD) models of neutral and mismatched cement mantle with dual-taper (top row) and triple-taper (bottom row) stems from superior and isometric views. DT, dual-taper; R, radius; TT, triple-taper.

for the purposes of FEA modelling. The contacting surface between the bone cement and the hip stem was defined as 'frictional', with a coefficient of friction 0.4 applied between surfaces.[12]

The components were meshed using quadratic elements with a size of 0.2 mm at the contacting surfaces. The mesh size was selected based on mesh independence test, showing that the von Mises stress did not vary when the mesh size was refined further than 0.2 mm at the contacting surfaces of both geometrical components, with the total number of nodes and elements being 1,225,526 and 715,312, respectively. A simulated axial force of 6,900 N in the -Z direction was applied at the proximal stem taper, with fixed supports employed at the distal end and outer shell of the cement mantle surface. This was chosen to represent stumbling force conditions estimated to be three times the standard loading condition,[24] and the maximum cyclic loading test is 2,300 N as per ISO standard for hip implants.[25] Simulation outputs included the von Mises stress (MPa) to observe stress distribution on the loaded components and indicate potential material yielding, maximum shear stress (MPa), and equivalent total strain (calculated from strain components/tensors along the X, Y, and Z directions), and directional deformations (mm) to assess subsidence in both the stem and cement models.[26,27] These results were used to compare the effect of varying contact areas (mm^2) from different mismatch positions. Additionally, the effect of subsidence on contact area for dual- and triple-taper stems (at neutral 0° and mismatched at 2.5° and 5° rotations) in both pre- and post-subsidence conditions were compared.

Results

Contact area model output

The relationship of surface area percentage in contact to the amount of rotation is illustrated in Figures 4 and 5 for dual- and triple-tapers, respectively. The contact model showed that there was a large decrease in surface contact area with even only a small rotation going from 100% at 0° to 50.00% at 2.5° for the dual-taper geometry, and from 100% at 0° to 50.20% at 2.5° for the triple-taper geometry. There was a gradual but small ongoing decrease in contact surface with increasing rotation for both the dual-taper and triple-taper geometries.

Effect of subsidence on contact area

The compensatory effect of subsidence is shown in Figure 6 for the dual-taper and Figure 7 for the triple-taper geometry. For both taper designs, there was an increase in contact surface area with an increase in subsidence. Similarly, the amount of contact surface area restored was also dependent on the taper angle, with larger taper angles restoring greater surface areas than smaller angles. The initial contact areas prior to any subsidence or load conditions for all variants of taper angles and mismatch rotational degrees were plotted as a baseline, generally around 50% of the full contact surface or slightly lower. In both taper geometry designs, the more the stems subsided into the cement mantle under loading, the more the contact surface was restored. Additionally, increasing the taper angle of the stem design increased the compensatory contact surface between the stem-cement interface under loading.

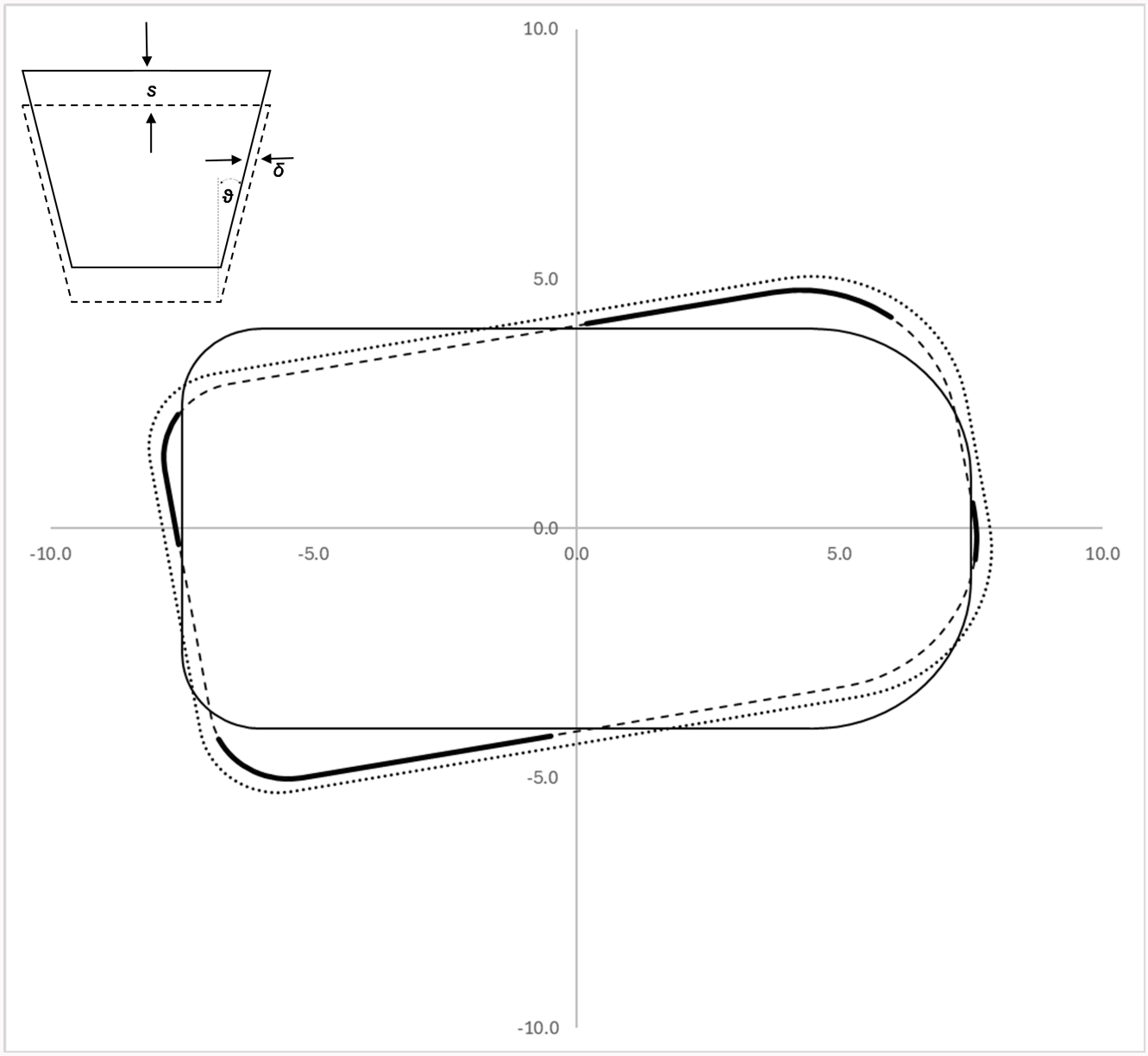

Fig. 3
Illustration to show relationship change in cross-sectional geometry (δ) with subsidence (s). The anterior-posterior view (inset) shows how with subsidence the cross-sectional profile will change with an increasing taper. The solid line represents the cement mantle, the bold lines represent the regions of the stem still in contact with cement, and the dashed lines represent the areas that are no longer in contact due to rotation prior to subsidence. The dotted line represents the cross-section of the stem post-subsidence, illustrating how this can increase the contact region.

Table I. Overview of the material properties used for each component of the finite element analysis model.[22,23]

Component	Material	Young's modulus, GPa	Poisson's ratio
Cement mantle	PMMA	2	0.3
Hip stem taper	Co-Cr alloy	220	0.3

Co-Cr, cobalt-chromium; PMMA, poly(methyl methacrylate).

Finite element model

The maximum output values resulting from the FEA simulations are shown in Table II, comparing the effect of reduced contact area at the stem-cement interface. In the 0° position, the triple-taper had a lower initial contact area than the dual-taper. Under mismatch conditions, the contact areas reduced, with the rotational 2.5° in dual and triple-taper stems dropping to 51.0% and 50.5%, respectively, of the full contact area. The contact areas further reduced when rotated by 5°, although the change was minimal (49.8% and 49.8%, respectively). This trend was similar to the outputs of the contact model (Figures 4 and 5). The contact areas in the contact model reduced under mismatch, with the rotational 2.5° in dual- and triple-taper stems decreasing to 49.1% and 49.4% of the full contact area, respectively. The contact areas also further dropped when rotated by 5° with minimal changes to 47.7% and 48.6%, respectively.

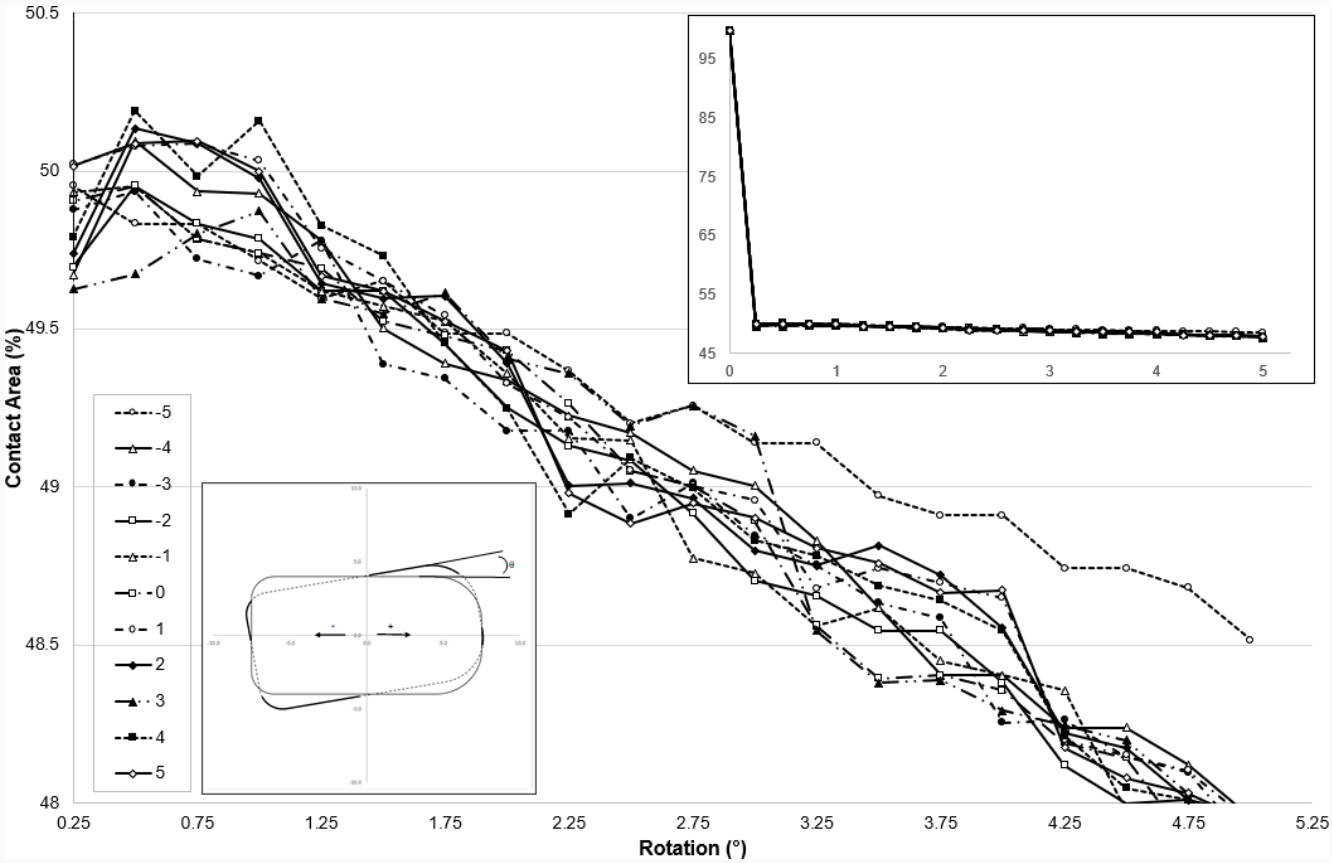

Fig. 4
The contact area percentages with rotation from 0.25° to 5° (0° to 5° see inset top right) and change in point of rotation in the x-axis from -5 mm to +5 mm (see inset bottom left) from centre for the dual-taper geometry.

With increasing mismatches and consequent contact area reduction, there was an increase in maximum stresses and total strain in the cement mantle. All triple-taper variants exhibited higher stresses and strains compared to the dual-tapers. An incremental stress of 51.4% was observed in the dual-taper's cement mantle when rotated by 2.5°, with only a slight further increase to 54.5% with a rotational mismatch of 5°. However, the incremental stress in the triple-taper's cement mantle was higher, with around 100.6% increase at 2.5° and 135.1% at 5°.

Figure 8 shows von Mises stress distribution (MPa) in the cement mantle. The von Mises stresses intensified at the distal section and the edges with smaller fillet radii, i.e. the lateral edges in the dual-taper and medial edge in triple-taper. Stress concentrations increased at the contact areas after the stems rotated, indicated by stress lines extending from the distal tip to each fillet corner and towards the midpoint of the broad surfaces. There was an increased stress region at the medial curved surface of the triple-taper's cement mantle under mismatch conditions, indicating higher von Mises stress. The highest maximum values of von Mises stress on the cement mantle were with a 5° rotation in both taper designs, reaching 68.29 MPa for dual-taper and 165.32 MPa for triple-taper.

The corresponding stresses in the stems are shown in Figure 9. After mismatch, stress areas were observed at six contact points in dual-tapers, with higher stress at the smaller radii. The medial surface of the triple-taper geometry showed increased stress. As with the cement mantles, the highest maximum values of von Mises stress on the stems were seen at 5° rotation, reaching 173.61 MPa for the dual-taper and 261.93 MPa for triple-taper geometries.

Shear stresses in the cement mantle were higher with triple-taper geometry compared to dual-taper stems (Figure 10). As seen in the cross-sectional anterior view, shear stresses were concentrated mostly at the distal end of the taper, extending proximally through the contacting areas of the implant-cement interface. The trend in shear stress distribution was consistent with the von Mises stress distribution in the cement component for all stem taper variants. As with the von Mises stress, the highest maximum values of shear stress on the cement mantle were observed with a 5° rotation, reaching 37.85 MPa for dual-taper and 92.09 MPa for the triple-taper.

Implant cement mantle mismatch approximately doubled the depth of subsidence for both dual- and triple-tapers in the 5° mismatch position, reaching 0.199 mm and 0.310 mm, respectively, compared to the 0° neutral stem position (0.096 mm for dual-taper and 0.146 mm for triple-taper stems) (Table III). As with subsidence, at 5° rotation, cement deformations doubled compared to the neutral position. The triple-taper geometry exhibited higher subsidence and cement mantle deformation compared to dual-taper stems. Cement deformation was greater on the medial aspect of the stem in triple-taper, corresponding to

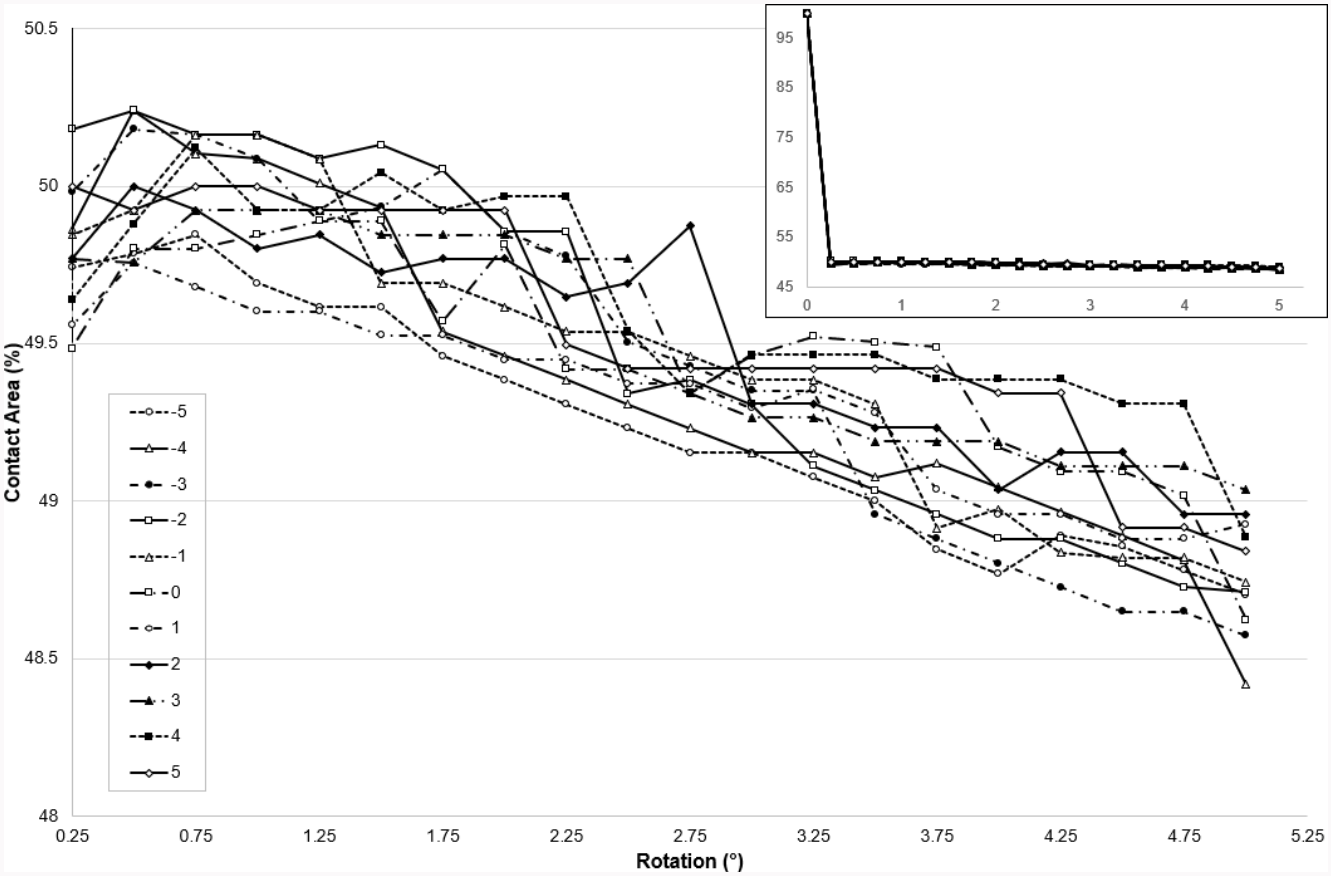

Fig. 5
The contact area percentages with rotation from 0.25° to 5° (0° to 5° see inset top right) and change in point of rotation in the x-axis from -5 mm to +5 mm from centre for the triple-taper geometry.

the increased stress in the cement mantle highlighting the influence of the cross-sectional geometry.

A comparison of the analytical and FEA models with reference to contact surface with subsidence is shown in Table IV. The FEA results showed a consistent trend with the results from the analytical model; however, the FEA results showed a more conservative increase in contact surface area with subsidence.

Discussion

The primary objective of this study was to investigate the hypothesis that a mismatch at the stem-cement interface contributes to increased pressure within the cement mantle of polished taper fit femoral stems, thereby potentially elevating the risk of PPFs post THA. A cross-sectional model was used to demonstrate the reduction in implant-cement contact area resulting from geometrical incongruity between the implant stem and the cement mantle. Subsequently, a finite element model was used to demonstrate the effects of reduced contact area due to implant-cement mismatch on stress distributions within the cement mantle under simulated loading conditions.

The effect of stem rotation on contact area showed that even minimal rotational movements resulted in a substantial loss of surface contact between the implant and the cement, as demonstrated through both numerical and FEA methods. This was the case for both the dual-taper and triple-taper geometries with contact at the implant-cement interface approximately halved with minimal rotation. Once rotated further, increase in rotation only resulted in small changes in the contact surfaces (Figures 4 and 5). There were relatively minor discrepancies between the two modelling approaches in the contact surface reduction results, only less than 1.4% for the dual-taper and less than 0.7% for the triple-taper models. However, these reductions in contact area validated a consistent trend of diminished interface integrity, as rotational mismatch increases were observed in both the contact model and the FEA. However, increased rotation did reduce the percentage contact restored through subsidence, with up to 5° rotational mismatch being compensated for with 2 mm of subsidence (Figures 6 and 7), although this effect was less pronounced when elastic deformation was taken into account in the FEA model (Table IV).

FEA simulations showed that the stress in the cement mantle increased with decreased contact at the implant-cement interface. The reduction in contact to 50.8% at 2.5° rotation resulted in an increase in von Mises stress to 151.4% for the dual-taper and 200.6% for the triple-taper cross-section. Under this extreme condition, which applied three times the standard load, the maximum von Mises stresses on the cement component, as shown in Table II, exceeded the yield strength of the PMMA cement material (29 MPa), indicating plastic deformation at the contacting surface of the cement.[22,23] In contrast, the maximum von Mises stresses on the stem component were lower than the yield strength of the Co-Cr alloy material (270 MPa). Similarly substantial increases

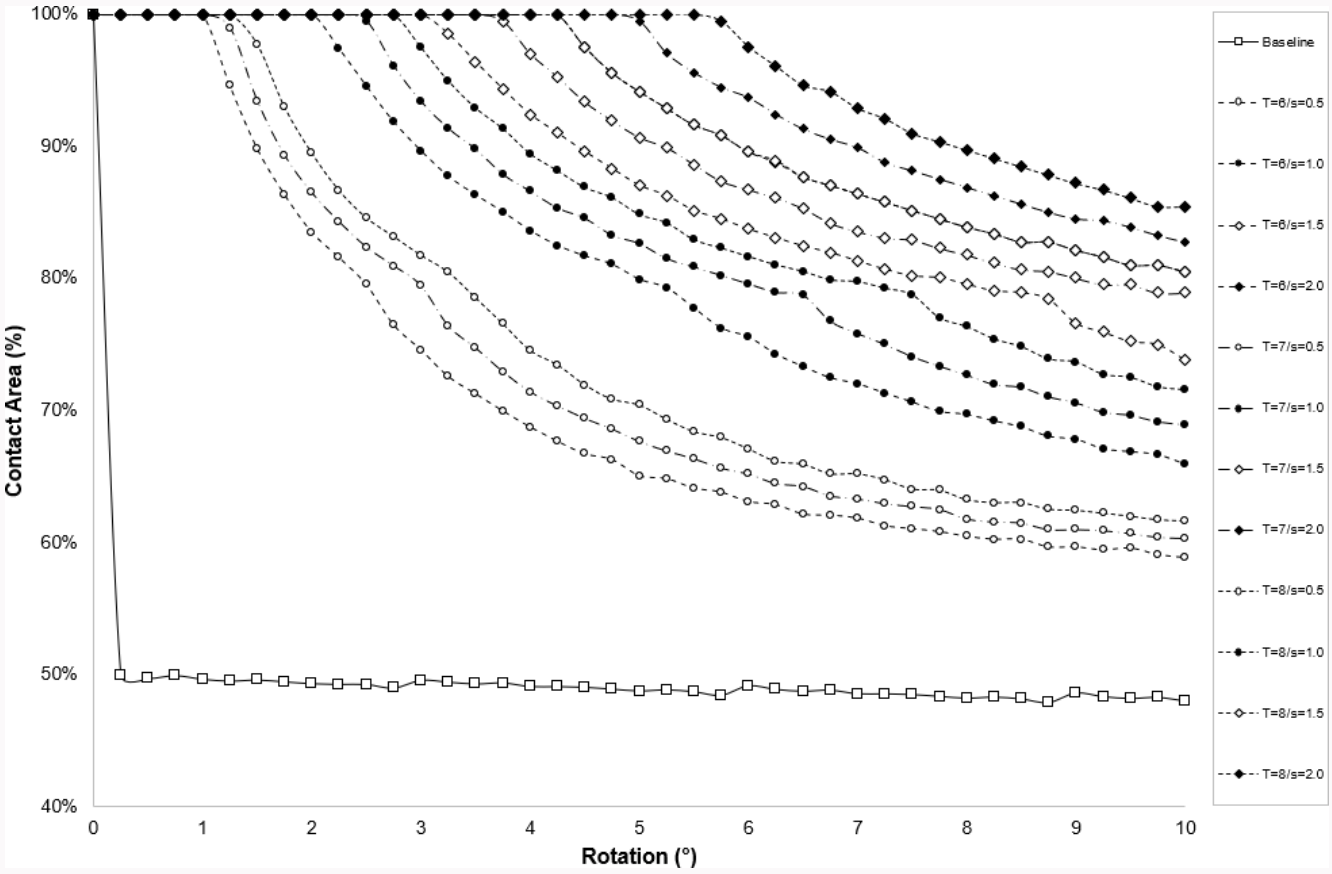

Fig. 6
The contact area percentage with rotation from 0° to 10° with series reflecting variation in both subsidence and taper for a dual-taper geometry.

in shear stress and total strains were also noted with decreased contact.

The substantial increase in stress and strain within the cement mantle with decreased contact highlights the importance of achieving an optimal implant-cement mantle interface. Although these findings do not directly link to the occurrence of PPFs, they do suggest that this mechanism could potentially play a contributory role to cement mantle failure and PPF among others. Optimizing the cement mantle at implantation should be a primary focus of the surgeon aiming to minimize relative movement of the implant while the cement is setting.

The compensatory mechanism of the stems when there was incongruity was demonstrated. The numerical model illustrated that subsidence could restore contact area in the event of a rotational mismatch. There was increased restoration of contact with increased subsidence; with 1° of rotational mismatch contact was restored with 0.5 mm subsidence increasing to contact for a 5° mismatch being restored with 2 mm subsidence (Figure 7). Similarly, the FEA simulations showed that under loading conditions, subsidence partially restored contact surface area at the implant-cement interface (Table IV). The absolute values for contact restoration were less for the FEA model, which is likely due to the fact that the FEA model more realistically took into account the material properties and contact friction, as opposed to the ideal frictionless conditions simulated in the numerical model. These findings illustrate the strength of the PTF design philosophy to compensate for implant-cement incongruency and resistance to loosening. The lower rates of loosening of PTF stems to other cemented designs have been documented previously.[3,28,29] However, this ability to maintain stem stability with subsidence does come with increased forces and increased peak stress and strain within the cement mantle.

The simulation presented in this paper is focused on the effect of an implant-cement interface mismatch during cementing, with unintended movement of the stem resulting in plastic deformation within curing cement. However, the mechanism of mismatch at the implant-cement interface may also occur later on in an implant's life cycle. Cement has been shown to fatigue and undergo plastic deformation with time.[16-18,30] With repeated rotational/torsional force and plastic deformation, a mismatch between cement mantle and implant will develop. The PTF mechanism compensates for this mismatch as subsidence of the stem can lead to increases in stresses and strains within the cement mantle, meaning it becomes increasingly susceptible to failure. An observed increase in the incidence of PPFs over time has recently been reported by Lynch Wong et al.[7] However, to validate this theory of fatigue-induced mismatch, further modelling and experimental studies would be required.

Although this work focused specifically on the implant-cement interface mismatch and the effect on the cement mantle, the effect of implant design in relation to the incidence of PPF is the subject of extensive debate.[4,31-33] Palan et al,[4] using registry data from England and Wales, reported that among the three most commonly used PTF designs, a triple-taper design had a lower risk of PPF requiring revision

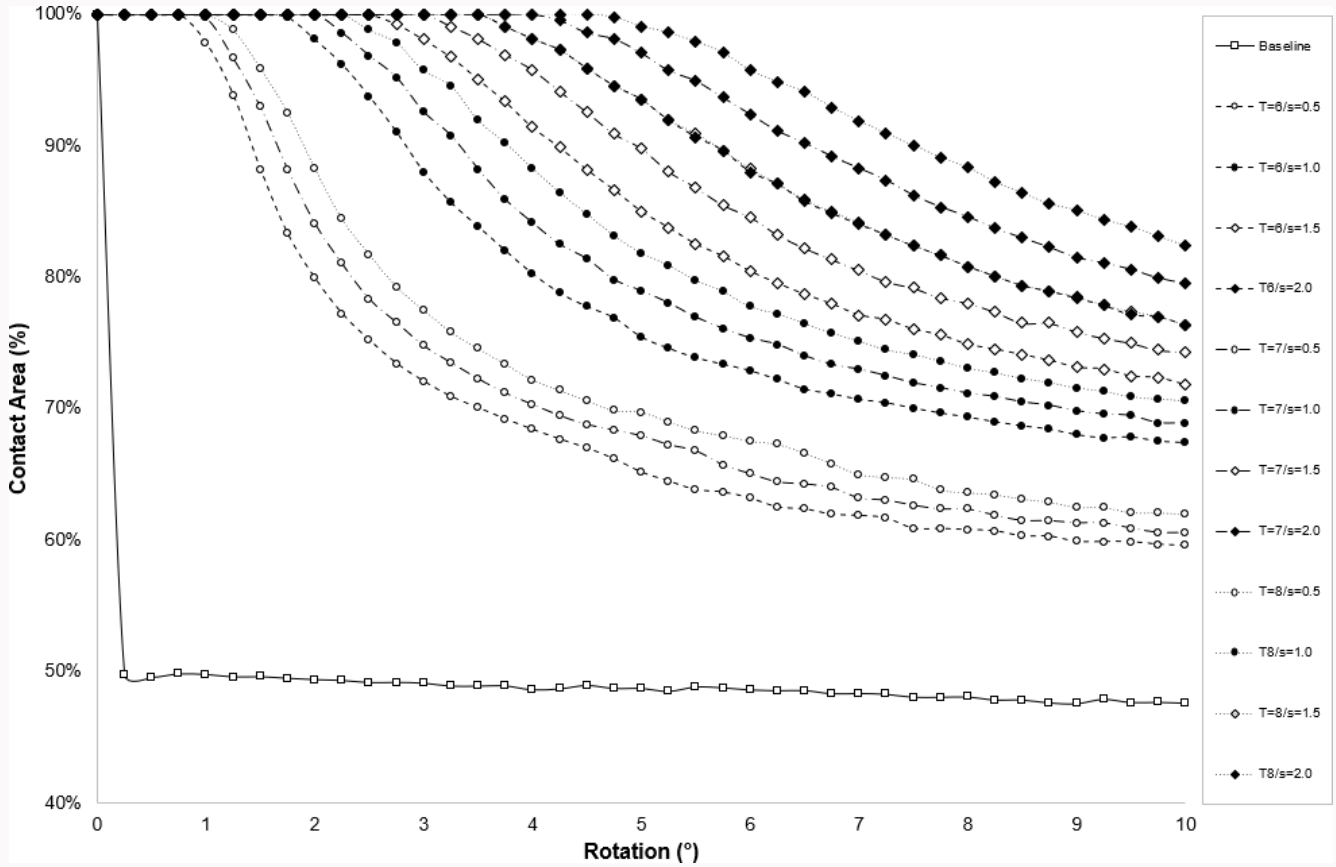

Fig. 7
The contact area percentage with rotation from 0° to 10° with series reflecting variation in both subsidence and taper for a triple-taper geometry.

Table II. Finite element analysis results on maximum (max.) stresses (MPa) and total strain following contact area changes of stem-cement interface in mismatches (2.5° and 5°) from the neutral position (0°). The percentage represents the ratio between the output values under each contact condition and the neutral condition (0°) for both dual- and triple-taper stems.

Hip stem taper	Contacting area, mm^2	Max. von Mises stress, MPa (Cement)	Max. von Mises stress, MPa (Stem)	Max. shear stress, MPa (Cement)	Max. total strain (Cement)
DT 0°	4,161.9 mm^2 (100%)	44.206 MPa (100%)	106.17 MPa (100%)	25.031 MPa (100%)	0.030368 (100%)
DT 2.5°	51.0%	151.4%	151.3%	140.8%	111.5%
DT 5°	49.8%	154.5%	163.5%	151.2%	131.3%
TT 0°	3,732.85 mm^2 (100%)	70.328 MPa (100%)	60.125 MPa (100%)	39.657 MPa (100%)	0.038142 (100%)
TT 2.5°	50.5%	200.6%	405.6%	209.1%	195.3%
TT 5°	49.8%	235.1%	435.6%	232.2%	229.8%

DT, dual-taper; TT, triple-taper.

in comparison to two dual-taper designs. Windell et al[31] tested two dual-taper designs and a triple-taper design in composite sawbone models, and found differences in torque to failure between designs where the triple-taper result was between the two dual-taper designs. Our findings showed increased stresses and subsidence with the triple-taper cross-section, which do not correspond with the clinical findings presented by Palan et al.[4] This is likely due to our use of estimated cross-sectional geometries for the two stem designs. In the models, the overall surface area for the triple-taper was less than the dual-taper, which would be reflected by an increase in contact pressures that is observed in our results. Additionally, our model did not take into account changes in stem length, which has been shown to influence the risk of PPF.[32] It is clear from our findings that smaller radii surfaces lead to increased contact forces and result in more rapid increases in contact force with implant-cement mantle mismatches. This aspect needs to be weighed against the need for smaller radii edges to provide torsional stability.

It is important to recognize the limitations of this study. First, it used simplified models. The cross-sectional geometries, although representative of existing stems, were not the exact

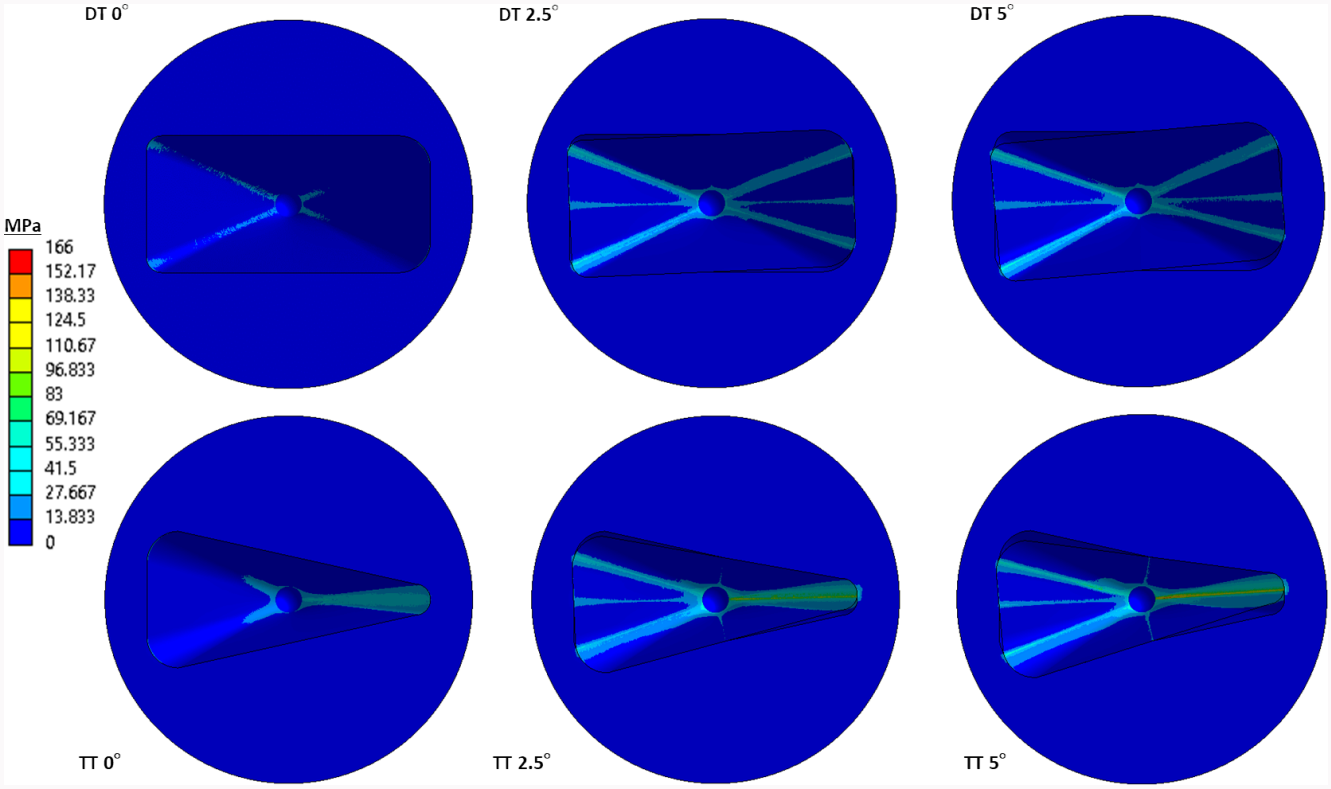

Fig. 8
Finite element analysis visualization from superior view on von Mises stress distribution (MPa) comparing cement mantles in neutral (0°) and mismatch positions (2.5° and 5°) for dual- and triple-taper stems.

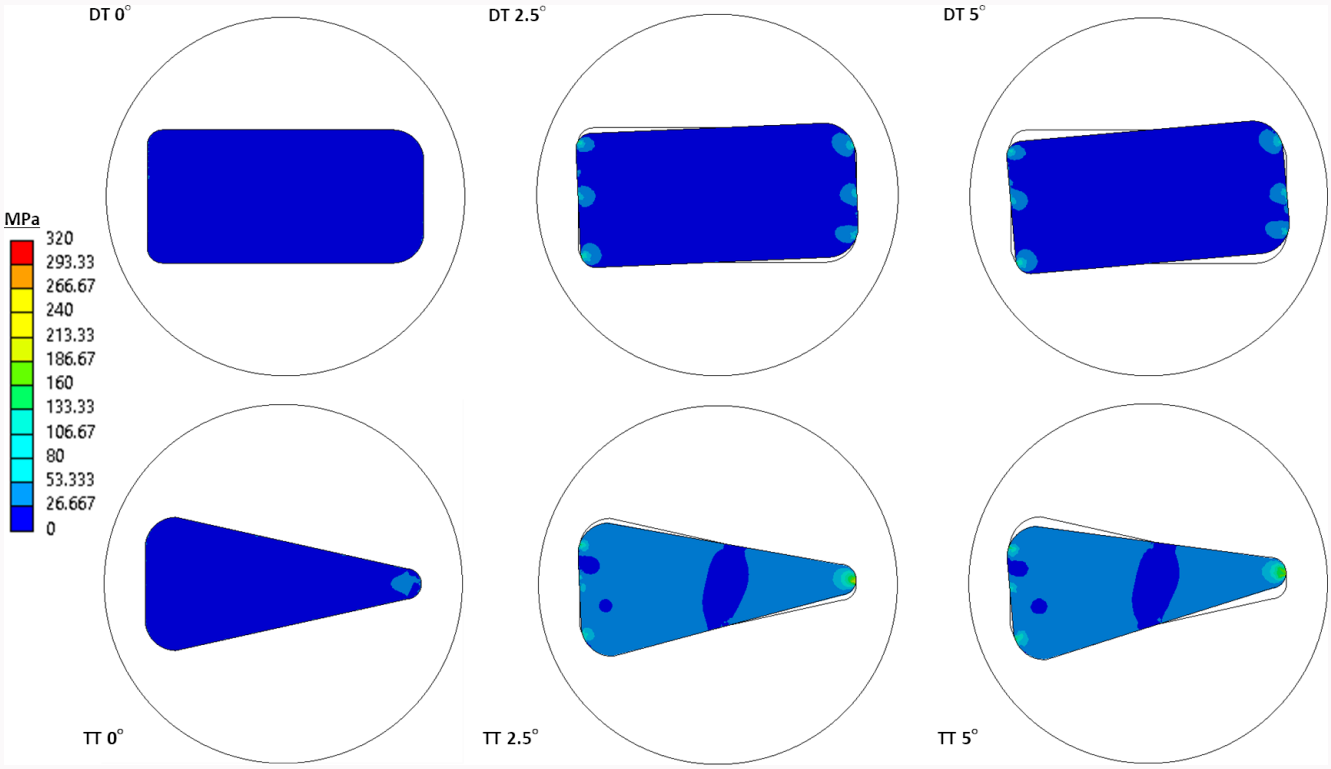

Fig. 9
Finite element analysis visualization from superior view on von Mises stress distribution (MPa) comparing cross-sectional stems in neutral (0°) and mismatch positions (2.5° and 5°) for dual- and triple-taper stems.

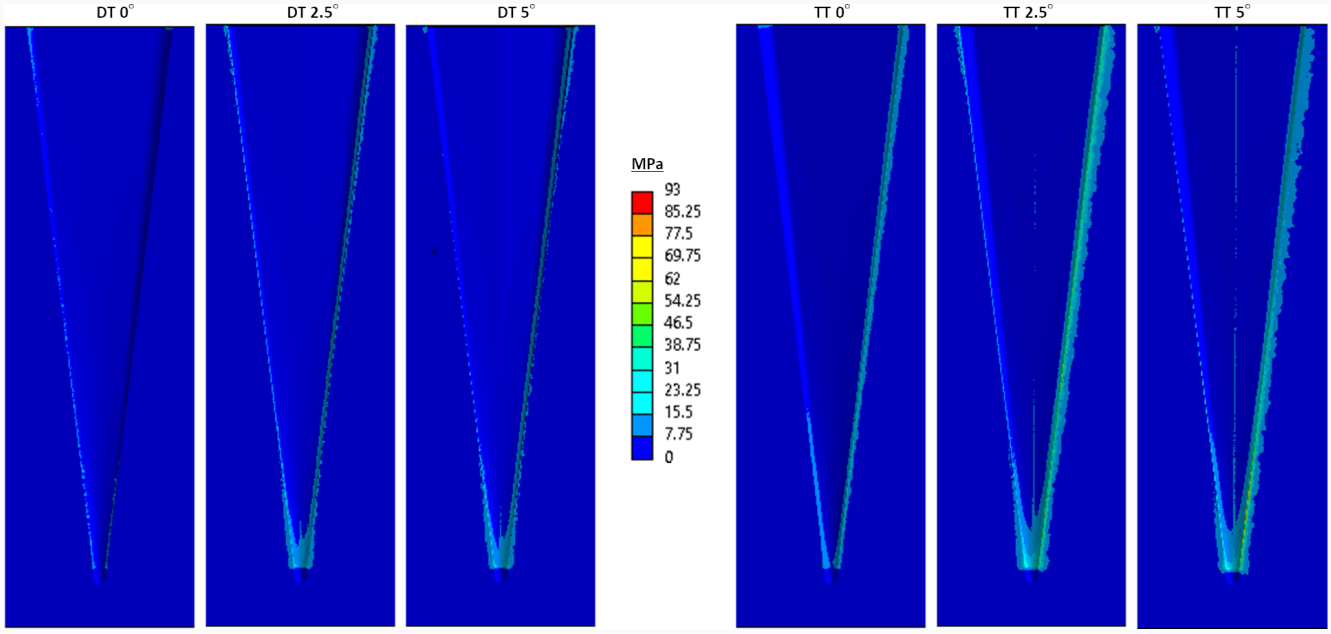

Fig. 10
Finite element analysis visualization from cross-sectional anterior view on maximum shear stress distribution (MPa) comparing cement mantles in neutral and mismatch positions for dual- and triple-taper stems.

Table III. Finite element analysis results on directional deformations of stem taper subsidence in -Z axis orientation and deformed cement mantle towards -/+ X-axis orientation both laterally and medially, taken from all converged stem taper simulations.

	S	δ_a	δ_b
Stem taper	**-Z Stem subsidence, mm**	**-X Cement lateral deformation, mm**	**+ X Cement medial deformation, mm**
DT 0°	0.096	0.013	0.010
DT 2.5°	0.191	0.018	0.019
DT 5°	0.199	0.019	0.020
TT 0°	0.146	0.009	0.021
TT 2.5°	0.324	0.022	0.045
TT 5°	0.310	0.027	0.048

DT, dual-taper; TT, triple-taper.

Table IV. Contact area percentage of stem-cement interface when unloaded (s = 0 mm) versus post-subsided (s = -0.5 mm) resulted from cross-sectional contact model and finite element analysis methods. Calculations for both geometries with a taper angle of 7°, and 0.5 mm subsidence.

	Contact area via numerical model		**Contact area via FEA**	
Stem taper	**Unloaded**	**Subsided (S = -0.5 mm)**	**Unloaded**	**Subsided (S = -0.5 mm)**
DT 0°	100%	100.0%	100%	100.0%
DT 2.5°	50.7%	82.4%	51.0%	67.7%
DT 5°	51.2%	67.7%	49.8%	57.2%
TT 0°	100%	100.0%	100%	100.0%
TT 2.5°	50.8%	78.3%	50.5%	58.0%
TT 5°	51.3%	67.9%	49.8%	51.6%

FEA, finite element analysis.

geometries of these stems. The model of the taper was simplified, whereas many implants make use of a complex taper. Furthermore, there can be variation in stem designs. Although the model used here did not make use of exact stem geometry, the geometries used were representative of the PTF stem principles. A linear load on the taper was used, which did not consider the more complex physiological loads seen in vivo. The point cloud numerical method used to determine contact surfaces potentially introduces errors, however these were marginal for small rotations (larger rotations were not modelled, as it is assumed that the occurrences of gross mismatches would be noticed and corrected by the surgeon) and we believed did not impact the interpretation of the outcomes. The FEA model implemented was a static calculation of a high-impact stumble which did not account for the time-dependent material behaviour of the cement. Additionally, this geometrical analysis did not consider the cyclical nature of loading with everyday activities. Indeed, in vivo the cement may undergo time-dependent change in its shape and structure after the stem is implanted, and this may alter the implant-cement interface including the extent of voids created. As such, this model is limited as it only modelled a single scenario (stumble), and did not account for fatigue of the implant or cement mantle with time under physiological conditions.

Overall, this study provides valuable insights into the mechanics of load transfer within the cement mantle and underscores the importance of interface integrity in the longevity and performance of PTF stems. Future research should continue to explore the interplay between stem design, cementing technique, and long-term clinical outcomes to develop more effective strategies for reducing PPF risk in THA procedures. Additionally, more in-depth modelling studies of stems in cement should be conducted to account for creep and plastic deformation, as well as rotational forces, to assess the impact of implant-cement interface secondary mismatch due to cement fatigue. In vitro testing would be the next step to be carried out to practically validate the surface contact mechanism by conducting load tests with controlled stem-cement positions inside femur samples.

In conclusion, this study highlights the importance of achieving an optimal implant-cement interface at the time of implantation. This places the onus on the surgeon to control factors that potentially lead to stem movement within the setting cement mantle, such as stem introducer removal, having an experienced assistant, and avoidance of last-minute adjustments. The mechanism of PTF stems compensates well for smaller mismatches; however, this comes with the trade-off of increased stresses in areas of the cement mantle which may compromise the long-term survival of the implant. Furthermore, although not the focus of this study, it is likely that rotational mismatches occur with cement fatigue due to torsional loads on the stem, resulting in a similar mechanism of compromise to the cement-mantle interface, leading to a potential increased risk of PPF.

Social media

Follow B. V. Bloch on X @Bloch_ortho, @NottsHipKnee

References

1. **Kayani B**, **Luo TD**, **Haddad FS**. Polished tapered stems in total hip arthroplasty: survival and risk factors for periprosthetic fractures. *Bone Joint J*. 2024;106-B(3):220–223.
2. **Kazi HA**, **Whitehouse SL**, **Howell JR**, **Timperley AJ**. Not all cemented hips are the same: a register-based (NJR) comparison of taper-slip and composite beam femoral stems. *Acta Orthop*. 2019;90(3):214–219.
3. **Heijnens LJ**, **Heyligers IC**, **Boonen B**, **Spekenbrink-Spooren A**, **van Haaren EH**, **Schotanus MG**. Survival rates of anatomically shaped and tapered slip cemented femoral implants: an analysis of 76,281 femoral implants of the Dutch arthroplasty register (LROI). *Hip Int*. 2023;33(6):1035–1042.
4. **Palan J**, **Smith MC**, **Gregg P**, **et al**. The influence of cemented femoral stem choice on the incidence of revision for periprosthetic fracture after primary total hip arthroplasty: an analysis of national joint registry data. *Bone Joint J*. 2016;98-B(10):1347–1354.
5. **Thien TM**, **Chatziagorou G**, **Garellick G**, **et al**. Periprosthetic femoral fracture within two years after total hip replacement: analysis of 437,629 operations in the nordic arthroplasty register association database. *J Bone Joint Surg Am*. 2014;96-A(19):e167.
6. **Jain S**, **Lamb JN**, **Pandit H**. Cemented femoral stem design and postoperative periprosthetic fracture risk following total hip arthroplasty. *Bone Joint J*. 2024;106-B(1):11–15.
7. **Lynch Wong M**, **Robinson M**, **Bryce L**, **et al**. Reoperation risk of periprosthetic fracture after primary total hip arthroplasty using a collared cementless or a taper-slip cemented stem. *Bone Joint J*. 2024;106-B(2):144–150.
8. **Kennedy IW**, **Meek RMD**. Latest developments in arthroplasty for hip fractures. *Bone Joint J*. 2024;106-B(12):1372–1376.
9. **Orce Rodríguez A**, **Smith PN**, **Johnson P**, **O'Sullivan M**, **Holder C**, **Shimmin A**. Registry-based study of survivorship of cemented femoral components versus collared cementless femoral components in total hip arthroplasty in older patients with osteoarthritis. *Bone Joint J*. 2024;106-B(3 Supple A):121–129.
10. **Jain S**, **Farook MZ**, **Aslam-Pervez N**, **et al**. A multicentre comparative analysis of fixation versus revision surgery for periprosthetic femoral fractures following total hip arthroplasty with a cemented polished taper-slip femoral component. *Bone Joint J*. 2023;105-B(2):124–134.
11. **Yagura T**, **Oe K**, **Kobayasi F**, **et al**. Experimental periprosthetic fractures with collarless polished tapered cemented stems. *Int Orthop*. 2024;48(5):1171–1178.
12. **Hirata M**, **Oe K**, **Kaneuji A**, **Uozu R**, **Shintani K**, **Saito T**. Relationship between the surface roughness of material and bone cement: an increased "polished" stem may result in the excessive taper-slip. *Materials (Basel)*. 2021;14(13):3702.
13. **Jain S**, **Lamb JN**, **Drake R**, **et al**. Risk factors for periprosthetic femoral fracture risk around a cemented polished taper-slip stem using an osteoporotic composite bone model. *Proc Inst Mech Eng H*. 2024;238(3):324–331.
14. **Lamb JN**, **Jain S**, **King SW**, **West RM**, **Pandit HG**. Risk factors for revision of polished taper-slip cemented stems for periprosthetic femoral fracture after primary total hip replacement: a Registry-Based Cohort Study from the National Joint Registry for England, Wales, Northern Ireland and the Isle of Man. *J Bone Joint Surg Am*. 2020;102-A(18):1600–1608.
15. **Shah N**, **Porter M**. Evolution of cemented stems. *Orthopedics*. 2005;28(8 Suppl):s819–25.
16. **Kim DG**, **Miller MA**, **Mann KA**. Creep dominates tensile fatigue damage of the cement-bone interface. *J Orthop Res*. 2004;22(3):633–640.
17. **Jeffers JRT**, **Browne M**, **Lennon AB**, **Prendergast PJ**, **Taylor M**. Cement mantle fatigue failure in total hip replacement: experimental and computational testing. *J Biomech*. 2007;40(7):1525–1533.
18. **Culleton TP**, **Prendergast PJ**, **Taylor D**. Fatigue failure in the cement mantle of an artificial hip joint. *Clin Mater*. 1993;12(2):95–102.
19. **Scheerlinck T**, **Casteleyn PP**. The design features of cemented femoral hip implants. *J Bone Joint Surg Br*. 2006;88-B(11):1409–1418.
20. **Verdonschot N**, **Huiskes R**. Femoral Stem Design and Cement Mantle Stress. In: Learmonth ID, ed. *Interfaces in Total Hip Arthroplasty*. London: Springer, 2000: 21–29.
21. **Baryeh K**, **Sochart DH**. Post-operative peri-prosthetic fracture rates following the use of cemented polished taper-slip stems for primary

total hip arthroplasty: a systematic review. *Arch Orthop Trauma Surg*. 2022;142(12):4075–4085.
22. **Nitoi D**, **Milicescu S**, **Apostolescu Z**, **Dimitrescu A**, **Chivu O**, **Teodorescu MC**. FEM of an implant behaviour in a healthy bone. *Procedia Engineering*. 2015;100:1092–1098.
23. **Soliman MM**, **Chowdhury MEH**, **Islam MT**, **et al**. A review of biomaterials and associated performance metrics analysis in pre-clinical finite element model and in implementation stages for total hip implant system. *Polymers (Basel)*. 2022;14(20):4308.
24. **Bergmann G**, **Graichen F**, **Rohlmann A**. Hip joint contact forces during stumbling. *Langenbecks Arch Surg*. 2004;389(1):53–59.
25. **K N C**, **Zuber M**, **Bhat N S**, **Shenoy B S**, **R Kini C**. Static structural analysis of different stem designs used in total hip arthroplasty using finite element method. *Heliyon*. 2019;5(6):e01767.
26. **Zulkifli AM**, **Shuib S**, **Sulaiman SH**, **Halim A**. IJTech - International Journal of Technology. Finite Element Analysis of Proximal Cement Fixation in Total Hip Arthroplasty. https://ijtech.eng.ui.ac.id/article/view/4318 (date last accessed 15 September 2024).
27. **Kaymaz I**, **Bayrak O**, **Karsan O**, **Celik A**, **Alsaran A**. Failure analysis of the cement mantle in total hip arthroplasty with an efficient probabilistic method. *Proc Inst Mech Eng H*. 2014;228(4):409–417.
28. **Hoskins W**, **van Bavel D**, **Lorimer M**, **de Steiger RN**. Polished cemented femoral stems have a lower rate of revision than matt finished cemented stems in total hip arthroplasty: an analysis of 96,315 cemented femoral stems. *J Arthroplasty*. 2018;33(5):1472–1476.
29. **Beksac B**, **Taveras NA**, **Valle AGD**, **Salvati EA**. Surface finish mechanics explain different clinical survivorship of cemented femoral stems for total hip arthroplasty. *J Long Term Eff Med Implants*. 2006;16(6):407–422.
30. **Takahashi E**, **Kaneuji A**, **Tsuda R**, **et al**. The influence of cement thickness on stem subsidence and cement creep in a collarless polished tapered stem: when are thick cement mantles detrimental? *Bone Joint Res*. 2017;6(5):351–357.
31. **Windell L**, **Kulkarni A**, **Alabort E**, **Barba D**, **Reed R**, **Singh HP**. Biomechanical comparison of periprosthetic femoral fracture risk in three femoral components in a sawbone model. *J Arthroplasty*. 2021;36(1):387–394.
32. **Morishima T**, **Ginsel BL**, **Choy GGH**, **Wilson LJ**, **Whitehouse SL**, **Crawford RW**. Periprosthetic fracture torque for short versus standard cemented hip stems: an experimental in vitro study. *J Arthroplasty*. 2014;29(5):1067–1071.
33. **Pakarinen OA**, **Neuvonen PS**, **Lainiala OS**, **Reito ARP**, **Eskelinen AP**. Periprosthetic femoral fracture is a leading cause of early revision with taper-slip stems in primary total hip arthroplasty: an analysis of 2765 total hip arthroplasties from a high-volume hospital. *J Arthroplasty*. 2021;36(11):3703–3708.

Author information

B. H. van Duren, DPhil, FRCS, Associate Professor in Orthopaedic Engineering, Leeds Institute of Rheumatic and Musculoskeletal Medicine, University of Leeds, Leeds, UK; Consultant Orthopaedic Surgeon,
Nottingham Elective Orthopaedic Services, Nottingham University Hospitals NHS Trust, Nottingham, UK.

M. Taufiqurrakhman, PhD, Research Fellow in Instrumented Implant Design
H. Pandit, DPhil, FRCS, Professor of Orthopaedics
Leeds Institute of Rheumatic and Musculoskeletal Medicine, University of Leeds, Leeds, UK.

A. Jones, PhD, Research Fellow in Instrumented Implant Design, School of Mechanical Engineering, University of Leeds, Leeds, UK.

M. Higgins, FRCS, Consultant Orthopaedic Surgeon
A. R. Manktelow, FRCS, Consultant Orthopaedic Surgeon
Nottingham Elective Orthopaedic Services, Nottingham University Hospitals NHS Trust, Nottingham, UK.

B. V. Bloch, FRCS, Consultant Orthopaedic Surgeon, Nottingham Elective Orthopaedic Services, Nottingham University Hospitals NHS Trust, Nottingham, UK; Honorary Assistant Professor, University of Nottingham, School of Medicine, Nottingham, UK.

Author contributions

B. H. van Duren: Conceptualization, Formal analysis, Investigation, Methodology, Project administration, Supervision, Validation, Visualization, Writing – original draft, Writing – review & editing.
M. Taufiqurrakhman: Formal analysis, Methodology, Writing – original draft, Writing – review & editing.
A. Jones: Writing – review & editing.
M. Higgins: Conceptualization, Writing – review & editing.
A. R. Manktelow: Conceptualization, Writing – review & editing.
B. V. Bloch: Conceptualization, Writing – review & editing.
H. Pandit: Resources, Supervision, Writing – review & editing.

Funding statement

The author(s) received no financial or material support for the research, authorship, and/or publication of this article.

ICMJE COI statement

The authors have no conflicts of interest to disclose. B. V. Bloch reports consulting fees from J&J MedTech, Solventum, and Zimmer Biomet, payment or honoraria for lectures, presentations, speakers bureaus, manuscript writing or educational events from J&J MedTech, and participation on a Data Safety or Monitoring Board or Advisory Board for J&J MedTech, all of which are unrelated to this study. B. V. Bloch also holds unpaid roles on the editorial boards of Bone & Joint 360 and KSSTA. M. Higgins reports consulting fees and payment for delivering lectures and cadaveric teaching at training events from Medacta International, unrelated to this study. A. Jones has received institutional research funding from DePuy Synthes, and is a co-investigator on an EPSRC / UKRI funded International Centre-to-Centre Grant project focused in part on hip replacement technology, as well as one of the work streams in the Leeds Biomedical Research Centre, all of which are unrelated to this study. A. Manktelow reports a design and royalty bearing contract with MatOrtho, royalties or licenses from Medacta, consulting fees and payment or honoraria for lectures, presentations, speakers bureaus, manuscript writing or educational events from Medacta, Zimmer Biomet, AO/DePuy Synthes, and MatOrtho, and support for attending meetings and/or travel from MatOrtho, Medacta, and Zimmer Biomet, all of which are unrelated to this study. H. Pandit reports institutional payments from DePuy Synthes, Zimmer Biomet, and Medacta International, consulting fees from DePuy Synthes, Zimmer Biomet, Medacta International, Allay Therapeutics, Paradigm pharmaceuticals, Microport, MATOrtho, and Invibio, and two patents related to SMART implants with the University of Leeds, stock or stock options in Allay Therapeutics, and receipt of equipment, materials, drugs, medical writing, gifts or other services from DePuy Synthes, Zimmer Biomet, Medacta International, Allay Therapeutics, Paradigm Pharma, and Pacira pharmaceuticals, all of which are unrelated to this study. B. van Duren reports research funding and receipt of equipment, materials, drugs, medical writing, gifts or other services from Medacta International, and is a named inventor on the patent for iSMART and its charging device, all of which are unrelated to this study.

Data sharing

The data that support the findings for this study are available to other researchers from the corresponding author upon reasonable request.

Acknowledgements

B. H. van Duren and H. Pandit are supported in part by the National Institute for Health and Care Research (NIHR) Leeds Biomedical Research Centre (BRC) (NIHR203331). The views expressed are those of the author(s) and not necessarily those of the NHS, NIHR, or Department of Health and Social Care.

Open access funding

The authors report that the open access funding for their manuscript was self-funded.